ARTICLE

From MoO_3 Nanobelts to MoO_2 Nanorods: Structure Transformation and Electrical Transport

Bin Hu,[†] Liqiang Mai,[†,‡] Wen Chen,[†,*] and Fan Yang[†]

[†]State Key Laboratory of Advanced Technology for Materials Synthesis and Processing, School of Materials Science and Engineering, Wuhan University of Technology, Wuhan 430070, China, and [‡]Department of Chemistry and Chemical Biology, Harvard University, Cambridge, Massachusetts 02138

ABSTRACT The MoO_2 nanorods (NRs) were synthesized by simple hydrogen reduction using the MoO_3 nanobelts (NBs) as the templates. The growth mechanism of one-dimensional (1D) MoO_2 nanostructure can be explained by the cleavage process due to the defects in the MoO_3 NBs. Different *I*/*V* characteristics of individual MoO_2 NRs were obtained at different bias voltages, which can be explained by Ohmic and Schottky conduction mechanisms, and the resistivity increased at high bias voltage probably because of the oxidation of MoO_2 NRs with large specific surface area.

KEYWORDS: MoO_2 · nanorods · structure transformation · reduction · cleavage · electrical · transport · oxidation

Developed techniques to control the size promote the potential application of molybdenum oxide in recent years.[1−3] Molybdenum oxide materials are particularly attractive among the transition-metal oxides due to their unusual chemistry produced by the multiple valence states. Nanostructured molybdenum oxide with high activity can be used in a wide variety of applications such as cathodes in rechargeable batteries, field-emission devices, solid lubricants, superconductors, thermoelectric materials, and electrochromic devices.[4−11] The molybdenum oxide crystal films may be used as solar cells and heated reflective films because of the favorable electrical properties.[12] The metals can be accessed in these molybdenum-based materials to form the stable coordination environments and have been used widely in the petrochemical industry for selective oxidation and isomerization of hydrocarbons.[13] Similarly, the shape of the nanocrystals is a crucial parameter in the determination of their properties.[14−16] The 1D nanostructures are ideal systems for investigating the dependence of electrical transport,[17] optical and mechanical properties on size and dimensionality.

Therefore, how to control the experimental conditions and select the suitable precursor for 1D molybdenum dioxide nanomaterial synthesis has attracted considerable attention. Until now, different methods to synthesize single-crystal MoO_3 NBs have been reported.[3,18−20] Although the MoO_2 NRs could be obtained under the reductive hydrothermal condition by *in situ* reduction based on α-MoO_3 NBs,[21] synthesis of the low valence state, metastable molybdenum dioxide in solutions is still a challenge. In addition, the strict selection of reducing agent, the high deficiency density, and amorphous phase of the final product need the improvement necessarily. Recently, we reported the electroactivity of MoO_3 NBs after lithiation that exhibits enhanced performance to nonlithiated MoO_3 NBs.[22] Herein, we introduce a simple and cost-saving method to transform MoO_3 NBs to 1D single-crystal MoO_2 NRs, and the possible growth mechanism is investigated. Furthermore, for application of MoO_2 nanostructures on various electronic devices, such as the printing of electronic device resistors with low temperature coefficients of resistance, we studied the electrical property through an individual MoO_2 NR to understand the electrical transport and interaction with metal contacts.

RESULTS AND DISCUSSION

X-ray diffraction (XRD) measurement was first used to study the phase change of the sample (Figure 1). The diffraction peaks of the XRD patterns for the sample before and after reduction can be readily indexed to be orthorhombic MoO_3 with preferred orientation (JCPDS No. 05-0508) in Figure 1A and monoclinic MoO_2 in space group $P2_1/c$ with the lattice constants of *a*

*Address correspondence to chenw@whut.edu.cn.

Received for review December 8, 2008 and accepted January 16, 2009.

Published online January 29, 2009.
10.1021/nn800844h CCC: $40.75

= 5.6 Å, b = 4.85 Å, c = 5.53 Å, θ = 119.37° (JCPDS No. 032-0671) in Figure 1B, respectively. No peaks of MoO_3 or other molybdenum oxides in Figure 1B are observed, indicating that MoO_3 was completely reduced to single-phase MoO_2.

The morphology of as-synthesized MoO_2 was characterized by scanning electron microscopy (SEM). Figure 2A gives the image of MoO_3 NBs, which were used as a template for MoO_2 NR synthesis. Low-magnification image of MoO_2 NR is shown in Figure 2B, and the NRs are observed decrease to 1−3 μm in length compared with 10 μm of MoO_3 NBs. The MoO_2 NRs are parallel to each other and indeed form bundles of agglomerated smaller filaments with diameters ranging from 100 to 200 nm, and high-magnification image gives more detail of morphology: the MoO_3 NB ruptured along the axial direction to form two paralleled MoO_2 NRs, as marked by the pane where the cleavage process can be seen clearly. Considering the drastic change of cell volume (34.5%) from MoO_3 (202.99 Å^3) to MoO_2 (130.52 Å^3), the surface of obtained MoO_2 NRs appears as saw-like edges as the arrowheads point at, and many short segments with lengths of 200−600 nm can be seen.

To determine the crystal structure of an individual MoO_2 NR, transmission electron microscopy (TEM) imaging and diffraction analysis were conducted. Figure 3A,B shows the TEM images of MoO_2 NRs with different surface morphology, and both of them are constituted of two paralleled NRs with different lengths, as shown in the SEM images. High-resolution transmission electron microscopy (HRTEM) images of MoO_2 NRs in Figure 3C,D show the 2D lattice fringes, and selected area electron diffraction (SAED) patterns further confirm that the NRs obtained by hydrogen reduction are single crystal. In fact, the data reveal that the MoO_2 NR is structurally uniform with interplanar spacings of approximately 0.34 and 0.28 nm corresponding to the (111) and (101) planes, respectively, and the growth direction is [012]. Unlike the porous structure synthesized by redox etching method in aqueous solutions,[21] the high-temperature reduction environment provided the sufficient thermal energy to remove the high-energy residual interface strain, which was caused by the lattice transformation, and it is thermodynamically favorable to form single-crystal MoO_2 NRs.

The following possible growth mechanism for the MoO_2 NRs in hydrogen gas is suggested: The structure of α-MoO_3 NB is anisotropic, which can be considered as a layered structure parallel to (010). Each layer is composed of two sublayers, each of which is formed by corner-shared octahedra along [001] and [100]; the two sublayers stack together by sharing the edges of the octahedra along [001]. An alternate stack of these layered sheets along [010] will lead to the formation of layered structure, where van der Waals interaction is the major binding between the piled sheets. The special structure features determine the formation of 1D MoO_2

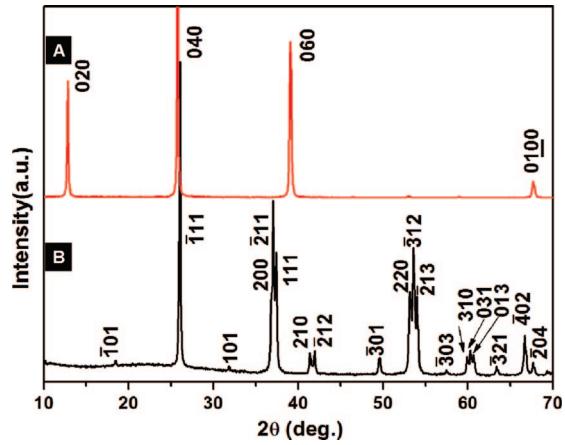

Figure 1. XRD patterns for the sample before (A) and after (B) reduction.

nanostructure, and the scheme of the cleavage process of MoO_3 NBs is shown in Figure 4A. Although the MoO_3 NBs were confirmed as single crystal by XRD and HRTEM, some defects such as oxygen deficiency and

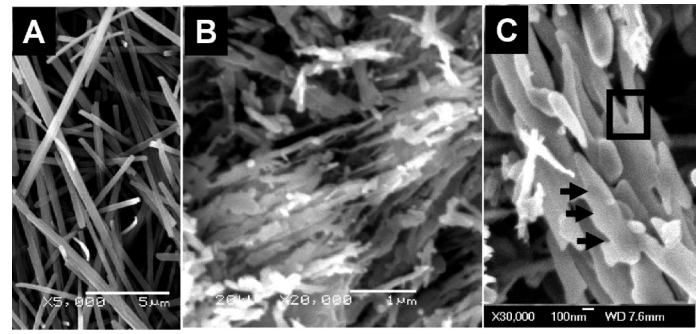

Figure 2. (A) SEM image of MoO_3 NB templates. (B) Low- and (C) high-magnification images of MoO_2 NRs.

dislocation are inevitable on the surface of MoO_3 NBs. These points with the lower activation energy can react with hydrogen preferentially.[23] Bond breaking along the [001] direction consumes less energy because only one Mo−O bond connects the corner-shared octahedral, while two Mo−O bonds connecting along the [100] direction need more energy to break. It is obvious that the cleavage along the axial direction of the nanobelts is much easier to carry out (Fig-

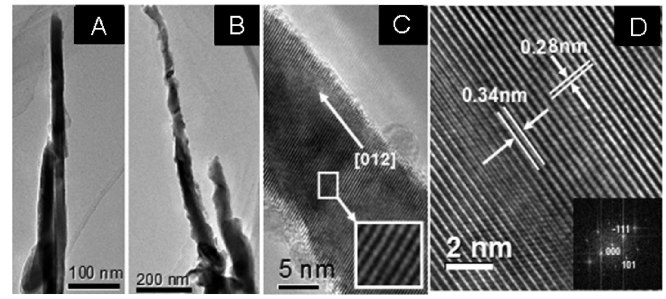

Figure 3. (A,B) TEM images of MoO_2 NRs with different surface morphology. (C) HRTEM image of MoO_2 NR growth along the [012] direction; the inset is an enlarged image of a representative portion of MoO_2 NR. (D) Clear lattice fringes of MoO_2 NR and the corresponding SAED image (inset).

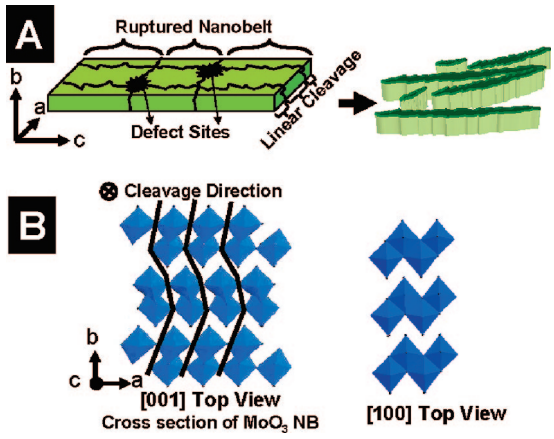

Figure 4. (A) Schematic illustration of the transformation from MoO_3 NB to MoO_2 NRs and (B) different top view of MoO_3 layered structure with the cleavage direction.

ure 4B), and distortion octahedra determine the appearance of the rough surface after cleavage, as shown in SEM and TEM images. Since catalytic, electrochromic, and photochromic gas-sensing properties of molybdenum oxides depend significantly on the surface state, the MoO_2 NRs with rough surface are promising for application of various fields, which is similar to the rough silicon nanowires applied in thermoelectric devices.[24]

Bulk MoO_2 with good electronic conductivity is a promising anode material in lithium secondary battery.[4] To understand the performance of nanoscaled MoO_2, we measured the electrical transport through individual MoO_2 NRs (Figure 5). The device was prepared by ac electrophoresis, and the contacts were improved through local deposition of Pt at the two ends by focused-ion-beam (FIB) microscopy, and the inset in Figure 5A shows the schematic view of the device.

The *I*/*V* characteristics were measured by sweeping the bias voltage from negative to positive for five times shown in Figure 5A,B,D. The obtained characteristic is symmetrical and behaves linearly dependent of *I versus V* in the low voltage range (Figure 5A), which is in agreement with Ohm's law as $E = J\rho$ or $V = IR$, where E, J, ρ, and R are the electric field, current density, resistivity, and resistance, respectively, and the voltage cycling scan for five times does not change the *I*/*V* curve. With the effective length and cross section of the sample at approximately 4 μm and 100 × 70 nm^2, respectively, the contact resistant is around 33 KΩ, and we can deduce the conductivity value as high as ~190 S/cm. This value can range from 80 to 400 S/cm depending on the different length, width, and thickness of the samples. Notably, the *I*/*V* hysteresis loop obtained in the figures shows weak memory effect, which is probably due to the electron charging effect.[25,26] All the results indicate that the low resistance, stable performance of a metallic MoO_2 NR is a good candidate material for electrical transport in the low electrical field.

When the bias voltage was up to 3 V, the conductivity of MoO_2 NR increased dramatically by 3 orders of magnitudes compared with that of MoO_3 NB (Figure 5B),[22] which is because the monoclinic MoO_2 is highly anisotropic and deviates only slightly from the rutile structure with strong Mo−Mo bonds, and the electronic properties are dominated by strong hybridization of O 2p and crystal field split Mo 4d states with bands near the Fermi energy originating almost exclusively from Mo 4d t_{2g} orbitals. Compared with the semiconductor MoO_3 with the band gap of 3.1 eV, the existence of delocalization electrons in the conduction band of MoO_2 accounts for the metallic property.

Unlike the feature in Figure 5A, the MoO_2 NR exhibits an exponential behavior in the current mechanism. The positive part of the *I*/*V* characteristics at the bias

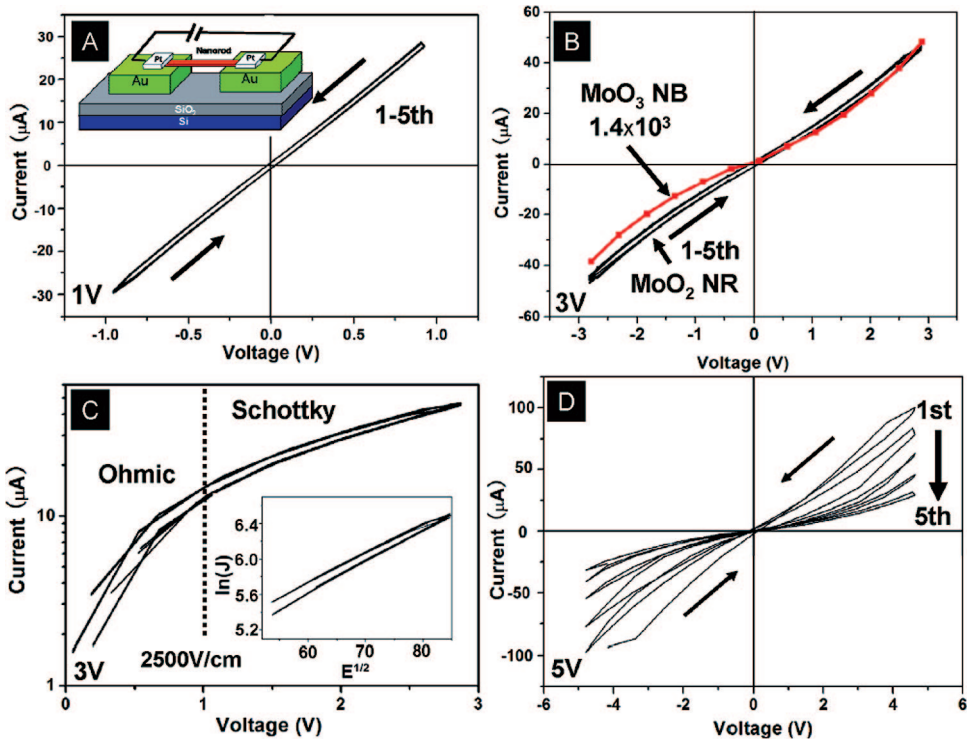

Figure 5. (A) *I*/*V* characteristics of individual MoO_2 NRs at 1 V. Inset: schematic view of individual nanorod device. (B) *I*/*V* curves of MoO_2 NRs and MoO_3 NBs at 3 V. (C) Positive part of the *I*/*V* characteristics of MoO_2 transversal system in panel B, rebuilt as a function of log(*I*). Inset: experimental plot of ln(*J*) *versus* $E^{1/2}$ at the electric field above 2500 V/cm. (D) Conductivity of MoO_2 NRs changed with the increase of the sweeping time at 5 V.

voltage of 3 V is shown in Figure 5C, rebuilt as a function of log(*I*). In order to determine the current mechanism in MoO_2 NR, the logarithm of the current density is plotted against the square root of the electric field [ln(*J*) *versus* $E^{1/2}$], as shown in the inset in Figure 5C. The linear feature obtained at the electric field above 2500 V/cm implies the Schottky emission, and the Schottky current density is expressed as follows:[17]

$$\ln J = \frac{\beta_{SE}\sqrt{E}}{kT} + \left[\ln(AT^2) - \frac{q\phi}{kT}\right] \quad (1)$$

where *A* is a constant, ϕ is the Schottky barrier height, *q* is the electronic charge, *k* is Boltzmann's constant, and *E* is the electric field.

In general, the device will be heated when the current flows across the nanomaterial and the calorific value is proportional to the current density, and the high working temperature will increase the conductivity of the nanodevice associated with the increased migration rate of carriers.[4,27] However, when the bias voltage further increased to 5 V, the *I*/*V* curve cannot be recovered with the process of sweeping, and the resistance increased slowly as shown in Figure 5D. Furthermore, the research shows that the effect of thermal annealing by the laser can oxidize the MoO_2 nanorods as MoO_x at threshold powers of 15 mW, and the *x* value can be controlled by the power of the laser.[28] Therefore, considering the metastable state of rough MoO_2 NR with high specific surface area, it is probable that the oxidation of MoO_2 to MoO_3 occurred due to the thermal effect by the high current density in the open condition, which decreased the conductivity finally.

CONCLUSIONS

Using MoO_3 NBs as the template, the MoO_2 NRs were obtained by hydrogen reduction, and the decrease of length and width can be explained by the cleavage mechanism because of the presence of the defects in the MoO_3 NBs. Ohmic characteristics as the dominant conduction mechanism at the electric field below 2500 V/cm is because of the existence of delocalizing electrons in the conduction band, and the conductivity of an individual MoO_2 NR is estimated to be 190 S/cm at room temperature, while the Schottky emission is responsible for the electric field above 2500 V/cm. With the large specific surface area, probably the MoO_2 NR was oxidized to MoO_3 when the device was heated at a higher current density, and the conductivity decreased slowly.

METHODS

To prepare the α-MoO_3 NBs, 40 mL of H_2O_2 (30%) was agitated rapidly, and 4 g of molybdenum powder was added slowly under water-cooling until the clear orange peroxomolybdic acid sol was obtained, then the sol was transferred into a Teflon-lined autoclave and kept at 180 °C for 48 h. The autoclave was left to cool, and the precipitate was filtered out and rinsed with deionized water three times. On the basis of the reduction of MoO_3 NBs with hydrogen gas, the pure MoO_2 NRs can been obtained successfully: 1 g of MoO_3 NB powder was sprinkled on an Al_2O_3 boat placed in a quartz chamber, and the argon gas was introduced into the chamber until heated to 550 °C at the heating rate of 10 °C · min^{-1}, then the hydrogen gas was injected into the chamber and held at 550 °C for half an hour; the powder cooled naturally in atmospheric argon flow, and finally, the blue MoO_3 transformed to black MoO_2 powder.

XRD measurement was performed using a D/MAX-III X-ray diffractometer. SEM images were collected with JSM-5610 and FES-EM LEO 1530. TEM, HRTEM, and SAED were recorded by a JEOL JEM-2010FEF microscope.

Acknowledgment. This work was supported by the National Nature Science Foundation of China (50672071, 50672072, 50702039), the Research Fund for the Doctoral Program of Higher Education (20070497012), Program for Changjiang Scholars and Innovative Research Team in University, Ministry of Education, China (PCSIRT, No. IRT0547). Thanks to Professor Z.L. Wang of Georgia Institute of Technology, Dr. C.S. Lao of California Institute of Technology for strong support and helpful discussion.

REFERENCES AND NOTES

1. Zhou, J.; Xu, N. S.; Deng, S. Z.; Chen, J.; She, J. C.; Wang, Z. L. Large-Area Nanowire Arrays of Molybdenum and Molybdenum Oxides: Synthesis and Field Emission Properties. *Adv. Mater.* **2003**, *15*, 1835–1840.
2. Sheehan, P. E.; Lieber, C. M. Nanotribology and Nanofabrication of MoO_3 Structures by Atomic Force Microscopy. *Science* **1996**, *272*, 1158–1161.
3. Li, X. L.; Liu, J. F.; Li, Y. D. Low-Temperature Synthesis of Large-Scale Single-Crystal Molybdenum Trioxide (MoO_3) Nanobelts. *Appl. Phys. Lett.* **2002**, *81*, 4832–4834.
4. Yang, L. C.; Gao, Q. S.; Tang, Y.; Wu, Y. P.; Holze, R. MoO_2 Synthesized by Reduction of MoO_3 with Ethanol Vapor as an Anode Material with Good Rate Capability for the Lithium Ion Battery. *J. Power Sources* **2008**, *179*, 357–360.
5. Liu, J. G.; Zhang, Z. J.; Pan, C. Y.; Zhao, Y.; Su, X.; Zhou, Y.; Yu, D. P. Enhanced Field Emission Properties of MoO_2 Nanorods with Controllable Shape and Orientation. *Mater. Lett.* **2004**, *58*, 3812–3815.
6. Tenne, R.; Margulis, L.; Genut, M.; Hodes, G. Polyhedral and Cylindrical Structures of WS_2. *Nature* **1992**, *360*, 444–446.
7. Arulraj, A.; Goutenoire, F.; Tabellout, M.; Bohnke, O.; Lacorre, P. Synthesis and Characterization of the Anionic Conductor System $La_2Mo_2O_{9-0.5x}F_x$ ($x = 0.02-0.30$). *Chem. Mater.* **2002**, *14*, 2492–2498.
8. Chevrel, R.; Hirrien, M.; Sergent, M. Superconducting Chevrel Phases: Prospects and Perspectives. *Polyhedron* **1986**, *5*, 87–94.
9. Caillat, T.; Fleurial, J. P.; Snyder, G. J. Potential of Chevrel Phases for Thermoelectric Applications. *Solid State Sci.* **1999**, *1*, 535–544.
10. McEvoy, T. M.; Stevenson, K. J.; Hupp, J. T.; Dang, X. J. Electrochemical Preparation of Molybdenum Trioxide Thin Films: Effect of Sintering on Electrochromic and Electroinsertion Properties. *Langmuir* **2003**, *19*, 4316–4326.
11. Bach, U.; Corr, D.; Lupo, D.; Pichot, F.; Ryan, M. Nanomaterials-Based Electrochromics for Paper-Quality Displays. *Adv. Mater.* **2002**, *14*, 845–848.
12. Nina, K.; Kimura, Y.; Yokoyama, K.; Kido, O.; Binyo, G.; Kaito, C. Direct Observation of MoO_2 Crystal Growth from Amorphous MoO_3 Film. *Physica E* **2008**, *40*, 2995–2998.

13. Okamoto, Y.; Oshima, N.; Kobayashi, Y.; Terasaki, O.; Kodaira, T.; Kubota, T. Structure of Intrazeolite Molybdenum Oxide Clusters and Their Catalysis of the Oxidation of Ethyl Alcohol. *Phys. Chem. Chem. Phys.* **2002**, *4*, 2852–2862.
14. Li, L. S.; Hu, J. T.; Yang, W. D.; Alivisatos, A. P. Band Gap Variation of Size- and Shape-Controlled Colloidal CdSe Quantum Rods. *Nano Lett.* **2001**, *1*, 349–351.
15. Hu, J. T.; Li, L. S.; Yang, W. D.; Manna, L.; Wang, L. W.; Alivisatos, A. P. Linearly Polarized Emission from Colloidal Semiconductor Quantum Rods. *Science* **2001**, *292*, 2060–2063.
16. Kovalenko, M. V.; Heiss, W.; Shevchenko, E. V.; Lee, J. S.; Schwinghammer, H.; Alivisatos, A. P.; Talapin, D. V. SnTe Nanocrystals: A New Example of Narrow-Gap Semiconductor Quantum Dots. *J. Am. Chem. Soc.* **2007**, *129*, 11354–11355.
17. Chakraborty, S.; Bera, M. K.; Dalapati, G. K.; Paramanik, D.; Varma, S.; Bose, P. K.; Bhattacharya, S.; Maiti, C. K. Leakage Current Characteristics and the Energy Band Diagram of $Al/ZrO_2/Si_{0.3}Ge_{0.7}$ Hetero-MIS Structures. *Semicond. Sci. Technol.* **2006**, *21*, 467–472.
18. Fang, L.; Shu, Y. Y.; Wang, A. Q.; Zhang, T. Green Synthesis and Characterization of Anisotropic Uniform Single-Crystal α-MoO_3 Nanostructures. *J. Phys. Chem. C* **2007**, *111*, 2401–2408.
19. Wang, S. T.; Zhang, Y. G.; Ma, X. C.; Wang, W. Z.; Li, X. B.; Zhang, Z. D.; Qian, Y. T. Hydrothermal Route to Single Crystalline α-MoO_3 Nanobelts and Hierarchical Structures. *Solid State Commun.* **2005**, *136*, 283–287.
20. Zhou, J.; Deng, S. Z.; Xu, N. S.; Chen, J.; She, J. C. Synthesis and Field-Emission Properties of Aligned MoO_3 Nanowires. *Appl. Phys. Lett.* **2003**, *83*, 2653–2655.
21. Wang, S. T.; Zhang, Y. G.; Wang, W. Z.; Li, G. L.; Ma, X. C.; Li, X. B.; Zhang, Z. D.; Qian, Y. T. Template-Assisted Synthesis of Porous Molybdenum Dioxide Nanofibers and Nanospheres by Redox Etching Method. *J. Cryst. Growth* **2006**, *290*, 96–102.
22. Mai, L. Q.; Hu, B.; Chen, W.; Qi, Y. Y.; Lao, C. S.; Yang, R. S.; Dai, Y.; Wang, Z. L. Lithiated MoO_3 Nanobelts with Greatly Improved Performance for Lithium Batteries. *Adv. Mater.* **2007**, *19*, 3712–3716.
23. Yang, L.; Yang, J.; Wang, Z. H.; Zeng, J. H.; Yang, L.; Qian, Y. T. Fabrication of Mesoporous CdS Nanorods by Chemical Etching. *J. Mater. Res.* **2003**, *18*, 396–401.
24. Hochbaum, A. I.; Chen, R. K.; Delgado, R. D.; Liang, W. J.; Garnett, E. C.; Najarian, M.; Majumdar, A.; Yang, P. D. Enhanced Thermoelectric Performance of Rough Silicon Nanowires. *Nature* **2008**, *451*, 163–168.
25. Kanoun, M.; Souifi, A.; Baron, T.; Mazen, F. Electrical Study of Ge-Nanocrystal-Based Metal-Oxide-Semiconductor Structures for p-Type Nonvolatile Memory Applications. *Appl. Phys. Lett.* **2004**, *84*, 5079–5081.
26. Schoen, D. T.; Xie, C.; Cui, Y. Electrical Switching and Phase Transformation in Silver Selenide Nanowires. *J. Am. Chem. Soc.* **2007**, *129*, 4116–4117.
27. Lin, Y. F.; Jian, W. B. The Impact of Nanocontact on Nanowire Based Nanoelectronics. *Nano Lett.* **2008**, *8*, 3146–3150.
28. Kumari, L.; Ma, Y. R.; Tsai, C. C.; Lin, Y. W.; Wu, S. Y.; Cheng, K. W.; Liou, Y. X-Ray Diffraction and Raman Scattering Studies on Large-Area Array and Nanobranched Structure of 1D MoO_2 Nanorods. *Nanotechnology* **2007**, *18*, 115717–115724.